Ionic Mobilities of Duplex and Frayed Wire DNA in Discontinuous Buffer Electrophoresis: Evidence of Interactions with Amino Acids†

Gregory M. K. Poon, Rashid M. Abu-Ghazalah, and Robert B. Macgregor, Jr.*

Department of Pharmaceutical Sciences, University of Toronto, Toronto, Ontario, Canada M5S 2S2

Received September 7, 2004; Revised Manuscript Received October 18, 2004

ABSTRACT: Nucleic acid−amino acid interactions are fundamental to understanding higher-order interactions made by nucleic acid-binding proteins. Here we employ electrophoresis to investigate DNA−amino acid interactions by using a set of amino acids (Ala, Gln, Gly, Met, Phe, Val, bicine and tricine) as trailing ions in a discontinuous buffer, and monitoring their interactions with duplex (from 12 to 3000 bp) and frayed wire [a set of self-assembled superstructures arising from d($A_{15}G_{15}$) oligodeoxyribonucleotides] DNA by the change in their ionic mobility (in terms of $\%R_f$) as a function of amino acid concentration in a polyacrylamide matrix. By titration of the pH of Tris-HCl polyacrylamide gels (from 7 to 10), a span of steady-state amino acid concentrations and extents of ionization can be maintained. We found that with a decrease in pH (thereby increasing amino acid concentrations and the extent of ionization of the α-amino group), both the $\%R_f$ and stacking limit were increased, but the extent varied among the trailing ions, resulting in an induced dispersion of $\%R_f$ values for a given analyte. Using singular-value analysis to take into account the $\%R_f$ dependence on fragment size (i.e., the $\%R_f$ distribution), the degree of dispersion was found to be positively correlated with the accumulation of N-protonated trailing ions in the resolving phase. These results indicate that the modification of $\%R_f$ of DNA is a mass-action effect involving DNA−amino acid interactions under essentially aqueous conditions.

As small ligands of nucleic acids, amino acids are of biological interest because of their connection to nucleic acid binding proteins and peptides. Over the years, nucleic acid interactions with amino acids and various derivatives in solution and the solid phase have been probed by a variety of spectroscopic techniques such as UV absorption, circular dichroism, fluorescence, and ^{1}H nuclear magnetic resonance (*1*−*10*). More recently, noncovalent interactions between amino acids and nucleic acid bases chemisorbed on solid surfaces have been studied by scanning tunnel microscopy (*11*). In solution, these interactions are relatively weak, nonspecific, and presumably electrostatic in nature (between the ligand's ammonium groups and the nucleic acid backbone), although intercalation by aromatic amino acids between nucleobases has also been described (*1*−*6*). Here we report a study of DNA−amino acid interactions by investigating the effect of amino acid association on the ionic mobilities of duplex and frayed wire DNA during electrophoresis in a polyacrylamide (PAA)[1] matrix. One advantage of analytical electrophoresis over spectroscopy is the ability to simultaneously study a complex mixture of DNA species (differing in size or structure, for example). In addition to their fundamental value, electrophoretic investigations are also valuable experimentally given the widespread interest in optimizing the resolution of analytes in genotyping studies by discontinuous buffer electrophoresis (*12*−*15*).

Our approach is to employ a discontinuous buffer PAA electrophoretic system with different amino acids as trailing ions and compare their effects on the $\%R_f$ distribution of duplex and frayed wire DNA. In a discontinuous buffer system, the concentration of the amino acid and its extent of ionization in the trailing phase (where electrophoresis of the analytes occurs) are governed by the ion concentrations in the leading phase, which are readily set by a suitable choice of leading and counterions (*16*). We used a Tris-HCl leading phase and adjusted the accumulation of the amino acid-trailing ions by titrating Tris to a pH range of 7−10 with HCl; the known concentrations of Tris and Cl^- in the leading phase then permit determination of the concentration of amino acids and pH in the trailing phase by applying multiphasic electrophoresis theory (*17*−*19*). Thus, we demonstrate that these amino acid-trailing ions give rise to a pH-dependent dispersion in the $\%R_f$ distribution that is graded with the accumulation of N_α-protonated amino acids in the trailing phase. In addition, we interpret the differences in the effect of amino acid interactions on the ion mobilities of duplex and frayed wire DNA in an attempt to further understand the structure and hydrodynamic properties of the latter noncanonical DNA isoform.

EXPERIMENTAL PROCEDURES

Materials. A duplex DNA (dsDNA) ladder was prepared by combining commercially available products (Fermentas SM0241 and SM0321; Fermentas, Vilnius, Lithuania) and

† This investigation was supported by grants from the Natural Science and Engineering Research Council to R.B.M. R.M.A.-G. was supported by a University of Toronto Open Fellowship.

* To whom correspondence should be addressed: Leslie Dan Faculty of Pharmacy, 19 Russell St., Toronto, Ontario, Canada M5S 2S2. Phone: (416) 978-5291. Fax: (416) 978-8511. E-mail: rob.macgregor@utoronto.ca.

[1] Abbreviations: FW, frayed wires; ODN, oligodeoxynucleotide; PAA, polyacrylamide; X, trailing ion; L_S, stacking limit in the resolving gel (phase π); R_f, retardation factor.

10.1021/bi0480786 CCC: $27.50
Published on Web 12/04/2004

synthetic oligodeoxyribonucleotides (ODNs). The fragment sizes (in base pairs) are as follows: 12, 80, 100, 200, 300, 400, 500, 600, 700, 800, 900, 1031, 1200, 1500, 2000, and 3000. Frayed wire (FW) DNA was prepared from d($A_{15}G_{15}$) as described previously (*20*). Various amino acids (glycine, L-alanine, L-valine, L-phenylalanine, L-glutamine, L-methionine, bicine, and tricine) and Bis-Tris were purchased from Sigma (Oakville, ON) or Fisher (Napean, ON) and were ≥98% pure. Acrylamide solutions (2.67% C), Tris, and other standard electrophoresis reagents were from Bio-Rad Laboratories (Hercules, CA). All solutions were prepared with Milli-Q deionized water (≥18.3 Ω·cm; Millipore, Billerica, MA).

Electrophoresis and Data Acquisition. Polyacrylamide electrophoresis was performed using a Hoefer SE-250 Mighty Small apparatus (Amersham Biosciences, Piscataway, NJ) essentially according to standard procedures. The gel cassette was 0.75 cm thick. Experiments were performed on either a single-phase 10.0% T gel containing 0.375 M Tris-HCl at various pH from 7 to 10, or a discontinuous Laemmli setup in which the resolving gel was cast to the height of 5.5 cm and topped with a 1 cm thick stacking gel (4.0% T) containing 0.125 M Bis-TrisHCl at pH 6.0 or 6.6 (depending on the calculated pI of the amino acid). Preliminary experiments had shown no discernible difference in the analytes' $\%R_f$ between the two modes of electrophoresis, although the addition of the stacking gel was greatly beneficial for resolution, especially for FW DNA. The running buffer consisted of 12.5 mM Tris base and 100 mM trailing ion without additional pH adjustment. Samples were diluted in a glycerol loading buffer (25%) containing 0.05% bromophenol blue, 0.05% orange G (Fisher), and 0.05% tartrazine (Sigma). The latter two tracking dyes were included because bromophenol blue (a monosulfonate, MW = 669) was not in all cases sufficiently mobile to mark the moving boundary. The more mobile orange G (a disulfonate, MW = 452) and tartrazine (a disulfonate-carboxylate, MW = 465) were added to correctly visualize the moving boundary.

Once the samples had been loaded, the gel was electrophoresed in a constant field of 15 V/cm until the dye-marked front had moved to within 1−2 mm of the bottom of the gel. Under this condition, ohmic heating was less than 5 °C from ambient temperature and the run lasted between 0.5 and 5 h depending on the resolving gel pH and the nature of the trailing ion.

Immediately after electrophoresis, the gel was stained with SYBR-gold (Molecular Probes, Eugene, OR) and digitized with a Storm 840 Imager (Molecular Dynamics, Sunnyvale, CA) at excitation and emission wavelengths of 450 and 520 nm, respectively, and a pixel resolution of 100 μm. Band detection and $\%R_f$ determination were performed with OneDScan software (Scanalytics, Fairfax, VA).

Numerical Analysis. Nonlinear curve fitting to empirical models employing the Marquart−Levenberg procedure was performed with Origin (Microcal, Northampton, MA). Expressed as a function of fragment size n (in base pairs for dsDNA or N for FW DNA oligomers), the $\%R_f$ distributions were fitted to biexponential functions of the form:

$$\%R_f = A_1 \exp\left(-\frac{n}{\tau_1}\right) + A_2 \exp\left(-\frac{n}{\tau_2}\right) + \%R_{f0} \quad (1)$$

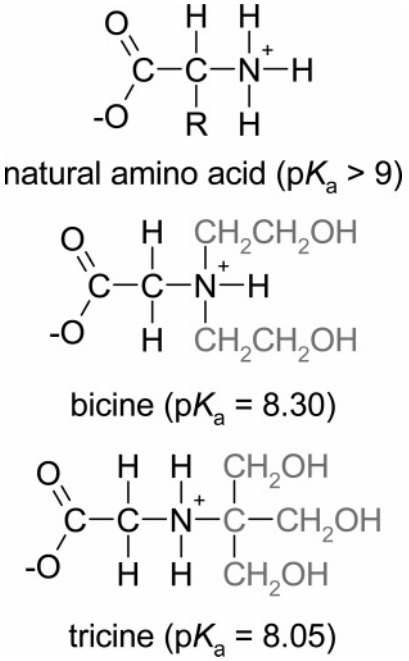

FIGURE 1: Structures of the amino acid trailing ions that were used. R denotes the usual side chains (e.g., R = H in glycine). Substitutions at the α-amino group in bicine and tricine are in gray. The pK_a values at 25 °C are also given.

where A_i, τ_i, and $\%R_{f0}$ are the estimated parameters. Alternatively, the data were fitted to a monoexponential relation by setting $|A_1| = |\tau_1| = 10^{-15}$ in eq 1. Goodness of fit was judged by χ^2 analysis with the number of degrees of freedom given by the relation $\nu = p - 1 - q$, where p is the number of observations and q is the number of fitted parameters.

RESULTS

Analysis of the Experimental System. We have deployed standard discontinuous buffer PAA electrophoresis with a variable running buffer and resolving gel pH to study the interactions of amino acid trailing ions with DNA by way of their effects on the DNA's size-dependent $\%R_f$. Six natural amino acids were studied in addition to bicine and tricine, which are N_α-substituted glycine analogues (Figure 1). The resolving gel contained 0.375 M Tris base titrated with HCl to a pH between 7 and 10, our operational variable, which in turn determined the leading ion (Cl^-) concentration:

$$[Cl^-] = \frac{c^\circ_{Tris}}{10^{pH^\lambda} - pK_a(Tris) + 1} \quad (2)$$

where $c^\circ_{Tris} = 0.375$ M. The running buffer consisted of 100 mM trailing ion and 12.5 mM Tris base; its unadjusted pH ranged from 7 to 8.5 depending on the identity of the trailing ion. Jovin (*17*−*19*, *21*) has demonstrated that it was neither necessary nor expedient to contrive conditions in the running buffer because, for a given trailing ion, the pH and concentrations of constituents in the trailing phase π[2] [in

[2] In the original presentation of the following relations, Jovin (*17*) had used the superscripts α and β instead of π and λ, respectively, as he was considering essentially a continuous gel. We make this substitution in keeping with his subsequent notation of a discontinuous slab system (*18*), which contains a stacking gel, as shown in Figure 2.

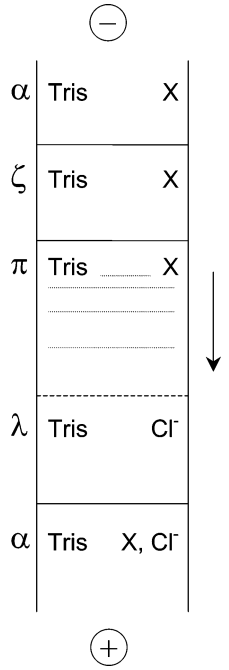

FIGURE 2: Schematic representation of our experimental multiphasic zone electrophoretic setup. Symbolic conventions of the phases are from Jovin (*19*), corresponding to the resolution stage. α represents the cathode (upper) and anode (lower) buffers which are constitutionally identical. Phase ζ is the stacking gel (when it is used) after the analytes have traversed through it. λ and π are the steady-state leading and trailing phases, respectively (demarcated by the moving boundary, dashes), of the resolving gel. The dotted lines represent sieving of the analytes in the homogeneous trailing phase π.

keeping with his notations (*18*, *19*); Figure 2] were completely determined by the constituents in leading phase λ (Figure 2). In some cases, we incorporated a stacking gel (phase ζ) to increase the band resolution and found no difference beyond experimental uncertainty (<5%) in the $\%R_f$ distribution from a continuous gel; hence, we neglect the effect of the stacking gel in the quantitative analyses that follow.

In a discontinuous electrophoretic system, the trailing ion front defines a moving boundary that discretely delimits the more mobile ion (Cl^- in our system) in phase λ and the less mobile trailing ion X^- in phase π (where resolution of the analytes occur). Maintenance of this moving boundary requires biased distributions of constituents and pH across the two phases (*17*):

$$\frac{c_X}{[Cl^-]} = \frac{1-\dfrac{\mu^\circ_{Tris}}{\mu^\circ_{Cl^-}}}{1-\dfrac{\mu^\circ_{Tris}}{\mu^\circ_{XH}}} \simeq \frac{1}{2}\left(1+\frac{\mu^\circ_{XH}}{\mu^\circ_{Cl^-}}\right) \qquad (3)$$

$$pH^\lambda - pH^\pi = \log\frac{\left(\dfrac{1}{\phi^\pi_{Tris}}-1\right)\left(1-\dfrac{\mu^\circ_{Tris}}{\mu^\circ_{XH}}\right)}{\left(\dfrac{\phi^\pi_X}{\phi^\pi_{Tris}}-1\right)\left(1-\dfrac{\mu^\circ_{Tris}}{\mu^\circ_{Cl^-}}\right)} < 0 \qquad (4)$$

where c_i denotes the concentration of constituent i (including all dissociated subspecies) and μ_i° and ϕ_i are the free ionic mobility and fractional ionization of i (see Table 1),

Table 1: Ionization and Mobility Properties of Selected Ions at 25 °C

ion	pK_a (α-amino)	pI[a]	free ionic mobility[b] μ° ($\times 10^{-8}$ m^2 s^{-1} V^{-1})
tricine	8.05	5.18	2.18
bicine	8.30	5.05	3.48
glycine	9.74	5.97	3.74
alanine	9.69	6.00	3.12
valine	9.61	5.96	3.01
phenylalanine	9.12	5.48	2.74
glutamine	9.13	5.65	2.97
methionine	9.20	5.74	3.1[c]
$TrisH^+$	8.07		2.60
Cl^-			8.05

[a] pI = ½[pK_a(α-carboxyl) + pK_a(α-amino)]. [b] Derived from Figure 4 of Jovin (*21*) or converted from diffusion coefficients D from Table 2p-4 of AIP (*33*) via the Einstein relation ($\mu RT = DF$). For the zwitterions, μ° is the limiting value for the −1 state. [c] Literature data are not available and approximated by the value for threonine.

respectively. The inequality in eq 4 implies that $pH^\pi > pH^\lambda$. Additionally, the differential concentrations of Tris and its trailing counterion in phase π impose a lower limit on the pH that is attainable:

$$pH^\pi > \frac{pK_a(TrisH^+) + pK_a(XH)}{2} \qquad (5)$$

The limiting value corresponds to $c^\pi_{Tris} = c^\pi_X$. As detailed by Jovin (*17*), the concentrations of Cl^- and Tris, the pK_a of Tris and the trailing ion, and the three constituents' free ionic mobilities μ° (Table 1) completely determine the pH and accumulation of Tris and the trailing ion in phase π (Figure 3), as well as their net mobilities (Figure 4). The resultant pH^π in turn determines the ionization and concentrations of the subspecies $[TrisH^+]^\pi$ and $[X\text{-}NH^+]^\pi$.

pH and Trailing Ions Conspire To Strongly Affect the $\%R_f$ Distribution of Duplex and FW DNA. A commercial dsDNA sizing ladder, prepared from the restriction digest of plasmid DNA, was used to calibrate the dependence of $\%R_f$ on chain length (in base pairs). The ladder contained essentially random sequence fragments (D. Morarescu, personal communication), and a 12 bp self-complementary sequence (5′-CGATACGTATCG-3′) was also included to afford a 3 log range in lengths (from 12 to 3000 bp).

To illustrate, electropherograms of the dsDNA ladder with glycine as the trailing ion are shown in Figure 5A. For all trailing ions, a decrease in the resolving gel pH (or equivalently, an increase in the Cl^- concentration and an attendant decrease in the net trailing ion mobility) increased the $\%R_f$ of dsDNA analytes (Figure 6A). This resulted in a pH-dependent dispersion in the $\%R_f$ distribution and, as reported previously (*16*), an increase in the stacking limit L_S, and separation of larger fragments. In our experiments, dsDNA fragments shorter than ~200 bp followed a significantly faster migration régime relative to larger fragments, and a biexponential function was required to fit the $\%R_f$ distributions ($p < 0.01$ vs a monoexponential fit).

Comparison among the trailing ions revealed that they did not disperse the $\%R_f$ distributions equally. Tricine and bicine had notably minor effects on the $\%R_f$ distribution compared to the natural amino acids, despite spanning a larger range in pH^π (Figure 3). The $\%R_f$ distributions for all the amino

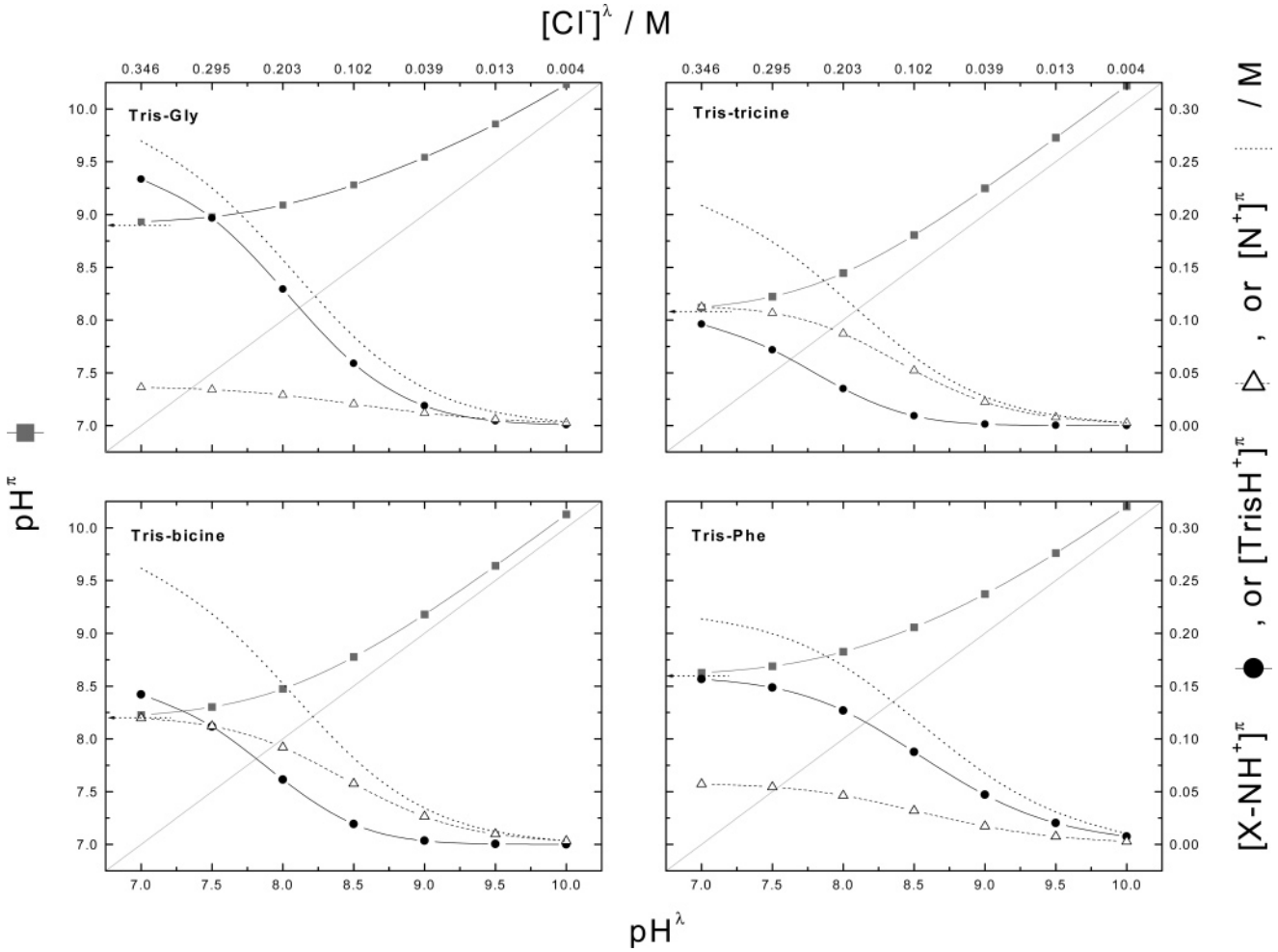

FIGURE 3: pH and concentration profiles of constituents in the resolving phase π as imposed by conditions set in the leading phase λ. The data are generated according to Jovin (*17*) using the pK_a values of the trailing ion and Tris and the $\mu°$ values of the trailing ion, Tris, and Cl^-. The dashed diagonal in each panel is the identity line to help show the positive pH bias in phase π by eq 4, and the pH^π is lower-bounded (dashed arrows) as prescribed by eq 5. The concentration profiles represent the protonated subspecies, i.e., $\phi_i c_i$, where $\phi_i = 10^{pK_a - pH}$ is the N_α-protonated fraction of constituent *i*. Because of their similar pK_a and $\mu°$ values, the profile for glycine is representative of alanine and valine, as is that of phenylalanine representative of methionine and glutamine.

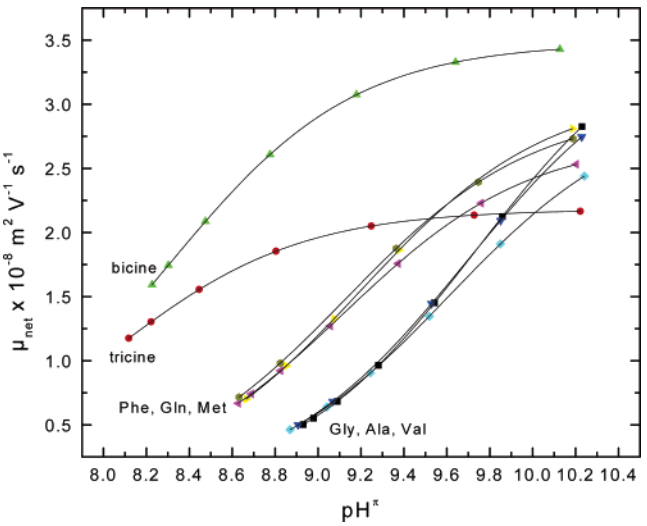

FIGURE 4: pH-dependent mobility profile of the trailing ions. The pH^π values indicated by the symbols were calculated as described in the legend of Figure 3. The net ionic mobility is calculated by the relation $\mu_{net} = (1 - \phi)_i \mu_i°$ from data in Table 1.

acids, however, converged at the highest pH^π that was tested (>10); the biexponential fits of the $\%R_f$ distributions for tricine, bicine, and glycine to eq 1 were statistically indistinguishable ($p < 0.05$) at pH^λ 10. Thus, with an increase in pH, ion-specific effects on the electrophoretic mobilities of dsDNA appeared to vanish. Importantly, the pH-dependent net mobilities of the trailing ions (Figure 4) did *not* converge in step with the observed $\%R_f$ distributions with an increase in pH. Control experiments without the use of a trailing ion (i.e., a continuous 0.375 M Tris-HCl gel) showed almost no effect on the dispersion in the $\%R_f$ distributions between pH 8 and 10. Thus, $TrisH^+$ ($pK_a = 8.07$) at up to 0.2 M exerted negligible effects on the $\%R_f$ of dsDNA analytes.

In addition to dsDNA fragments, the effects of amino acid trailing ions on the $\%R_f$ of d($A_{15}G_{15}$) oligomers were investigated (Figure 6B). ODNs such as this containing long terminal runs of consecutive guanine residues spontaneously self-assemble to form polydisperse superstructures called DNA frayed wires (FW) (*20*, *22*−*28*). These structures consist of two distinct conformational domains: a guanine stem arising from guanine−guanine interactions that hold the DNA strands together and an "arm" domain whereby the single-stranded non-guanine portion of the parent ODNs protrudes out of the guanine-rich core (hence the term "frayed"). When separated by electrophoresis, these highly

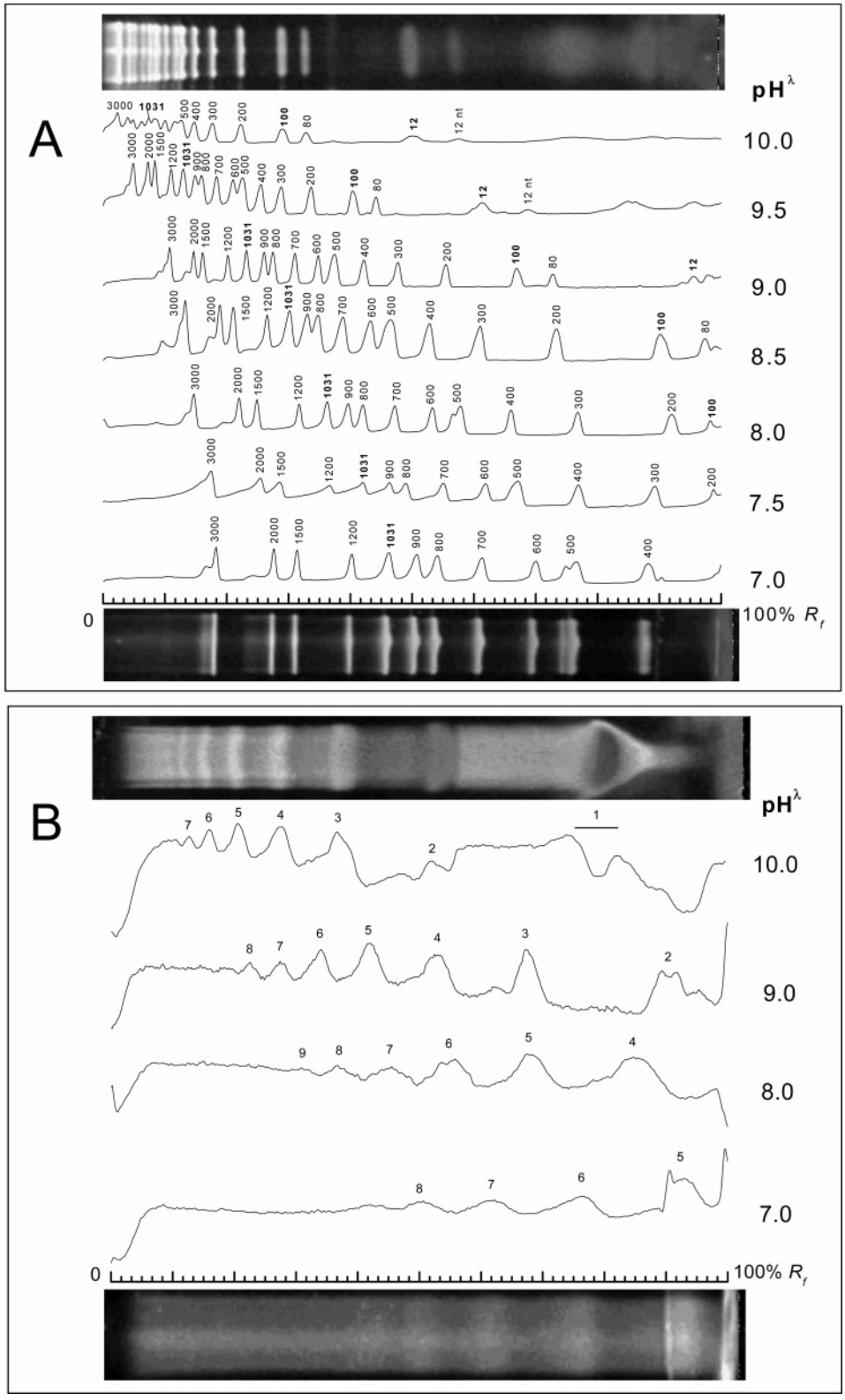

FIGURE 5: Electropherograms for DNA with glycine as the trailing ion at pH$^\lambda$ 7−10. The direction of electrophoresis is from left to right. The SYBR-gold-stained gel images for runs at the lowest and highest pH$^\lambda$ (7 and 10, respectively) are also shown. (A) dsDNA. Labels indicate the fragment size in base pairs; approximate order-of-magnitude markers are in bold. (B) Frayed wire DNA. Labels indicate the *N*th oligomer. The monomer at pH$^\lambda$ 10 appeared as a trough due to an inner filter effect arising from overstaining.

stable species form a characteristic ladder of bands each differing by a single strand (*20*). Given their unique structures, FW DNA provided another avenue for studying trailing ion−DNA interactions in PAA gels.

The %R_f distributions of FW DNA are expressed in terms of the *N*th oligomer (Figure 6B). Except for the monomer ($N = 1$), FW DNA exhibits a lower mobility than dsDNA with an equivalent molecular weight (*23*). In general, FW DNA did not resolve as well as dsDNA due to the broader bandwidths of FW bands and greater background staining, although the resolution was greatly enhanced by the use of a stacking gel. Fewer bands could be resolved at low

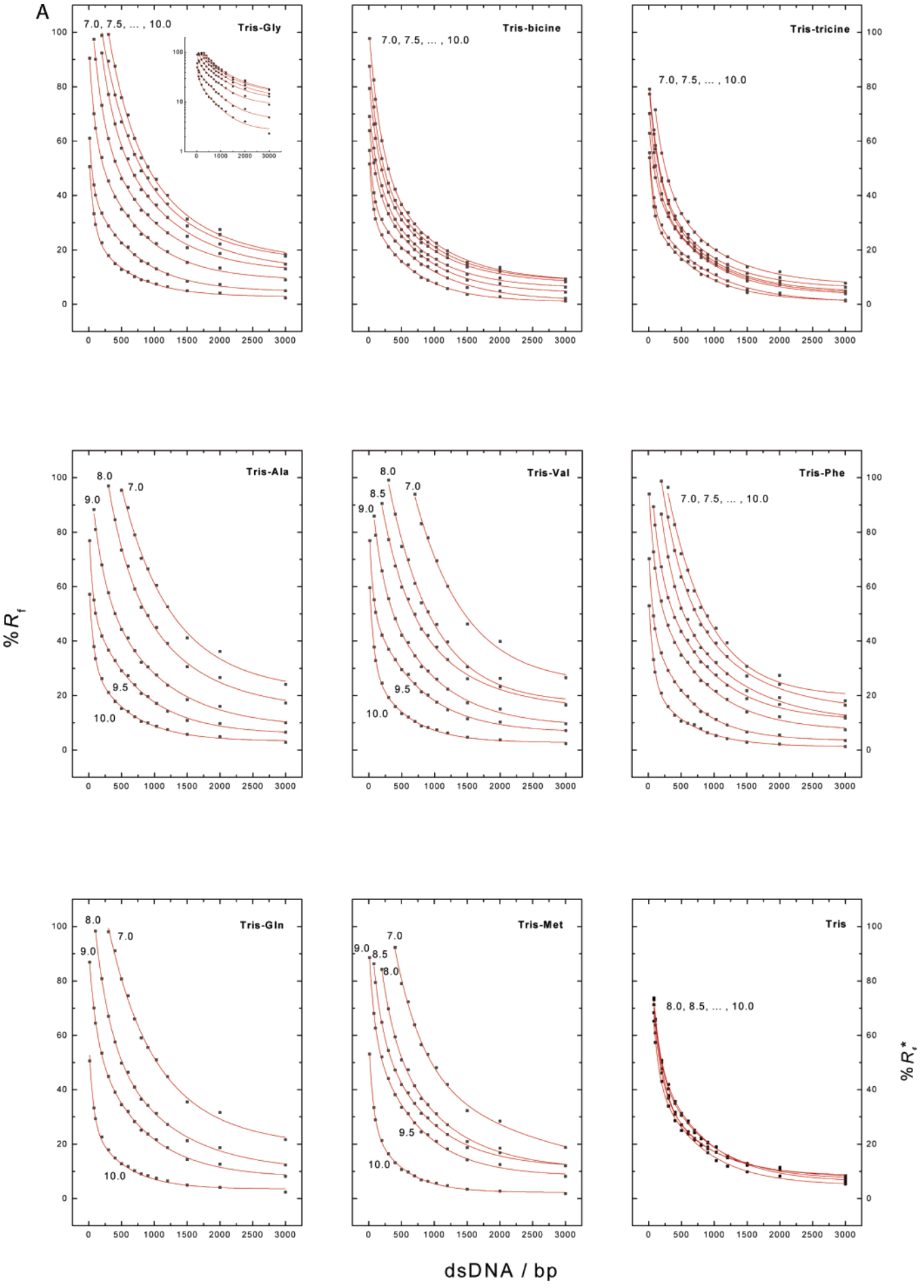
A
Tris-Gly
7.0, 7.5, ... , 10.0
Tris-bicine
7.0, 7.5, ... , 10.0
Tris-tricine
7.0, 7.5, ... , 10.0
Tris-Ala
8.0
7.0
9.0
9.5
10.0
Tris-Val
8.0
7.0
8.5
9.0
9.5
10.0
Tris-Phe
7.0, 7.5, ... , 10.0
Tris-Gln
8.0
7.0
9.0
10.0
Tris-Met
7.0
9.0
8.5
8.0
9.5
10.0
Tris
8.0, 8.5, ... , 10.0
%R_f
%R_f^*
dsDNA / bp

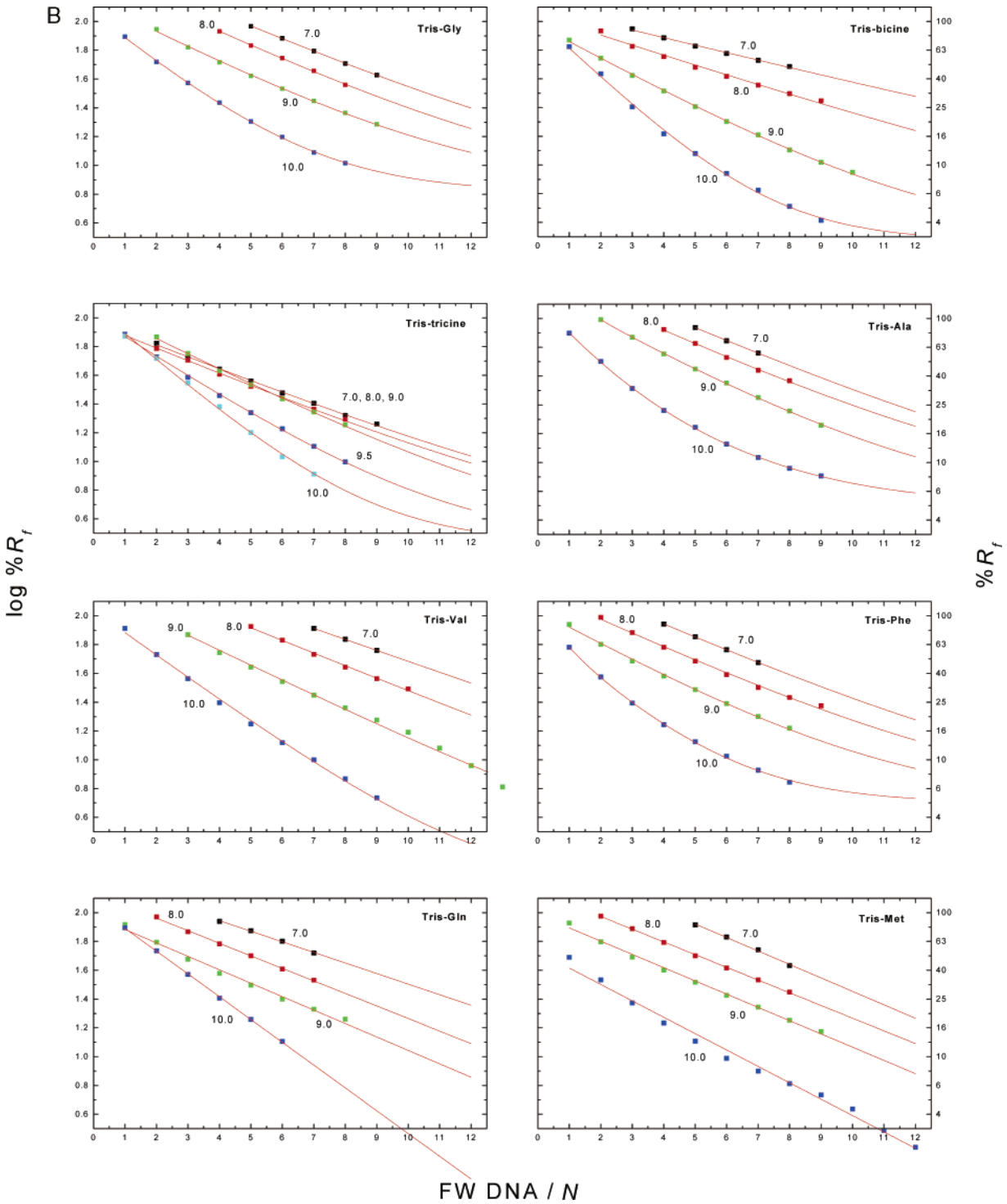

FIGURE 6: %R_f distributions for DNA in a discontinuous buffer Tris-HCl gel with various amino acids as the trailing ion. %R_f was measured relative to the steady-state moving boundary. Lines are global fits to eq 1 for each trailing ion. Labels indicate the pH^{λ} at which the experiments were performed; the corresponding pH^{π} values are higher (eq 4). Analyses of replicate experiments and %R_f determinations indicate an average error of ~5%. (A) dsDNA. For the Tris-only experiments (bottom right panel), %R_f* was taken relative to the 12 bp fragment as they were continuous systems with no ion front. The inset in the Tris-glycine panel redraws the data on a log %R_f scale. (B) FW DNA. Note that log %R_f is plotted on the ordinate, against oligomeric state N. Fitted lines are extended to an N value of 12 to indicate the relative resolution of bands among trailing ions and conditions.

resolving gel pH, and the amino acid that was used also appeared to be a mitigating factor: glutamine, for example, gave particularly poor resolution, while methionine afforded the highest signal-to-noise ratio. All the %R_f distributions were described well by a monoexponential fit (the curvatures seen in some log %R_f vs N plots are due to non-zero values of %R_{f0}). Qualitatively, resolving gel pH produced the same effects on the %R_f of FW DNA as dsDNA: %R_f increased for any given N with progressive stacking of smaller oligomers as the pH decreased. The extent to which this occurred, as for dsDNA, varied significantly among the trailing ions. The %R_f dispersion was particularly severe with valine, whereas tricine produced approximately identical %R_f distributions from pH^{λ} 7 to 9. Although the dispersion

produced by bicine was comparable to those of the natural amino acids, the increase in the stacking limit at pH^{λ} 7 ($L_S = 3$) was higher only than that of tricine ($L_S = 2$). Overall, compared to that of dsDNA, the $\%R_f$ dispersions produced by the trailing ions were more heterogeneous, but the $\%R_f$ distributions at pH^{λ} 10 were qualitatively similar.

No Other Buffer or Electrical Parameters Exerted Significant Effects on the $\%R_f$ Distribution. In addition to the identity of trailing ion and pH^{π}, we sought other experimental parameters that might affect the $\%R_f$ of DNA analytes. Only variations in the sieving matrix itself, namely, the concentration of PAA (%T) and degree of cross-linking (%C), had significant effects on the $\%R_f$ (data not shown). The concentration of the trailing ion had a moderate effect on the run time and current flow but was otherwise inconsequential to $\%R_f$, consistent with the constraints imposed by the steady-state moving boundary (*17*, *29*). Glycine, for instance, yielded the same $\%R_f$ distribution for all analytes at pH 9.0 across a concentration range from 100 to 400 mM (data now shown). Similarly, variations in the electric field (e.g., constant voltages from 10 to 25 V/cm or currents from 10 to 20 mA with voltages peaking above 45 V/cm) yielded indistinguishable $\%R_f$ curves. The field strength of 15 V/cm was chosen to provide a convenient run time without excessive ohmic heating in the gel.

DISCUSSION

The fascinating effects of trailing ion identity and resolving gel pH on the $\%R_f$ distribution of dsDNA were first described by Doktycz (*16*). We have significantly extended this line of investigation by studying the differential dispersion of the $\%R_f$ distributions of duplex and FW DNA by a series of amino acids across a range of pHs.

In the analysis of the $\%R_f$ distributions, direct fitting to empirical functions (such as exponentials) is of limited utility in the absence of a mechanistic model. In this regard, singular-value decomposition (SVD) is an elegant alternative that considers the $\%R_f$ line shape throughout the experimental range of fragment sizes without prejudice to mechanism. Thus, aggregate $\%R_f$ values obtained at each resolving gel pH for all amino acids were organized as column vectors $\mathbf{x}_k$ (48 in total) in the source matrix $\mathbf{X}$ and decomposed into the product

$$\mathbf{X} = \mathbf{USV}^T \tag{6}$$

$\%R_f$ values for fragment sizes that were not destacked in phase π under a given condition were set to 100%. The column eigenvectors vectors $\mathbf{u}_j$ are the basis $\%R_f$ curves; linear superposition of these basis curves yields the observed $\%R_f$ profiles. The $\mathbf{v}_k$ column gives the amplitudes corresponding to the basis curves as a function of the corresponding experimental condition k (trailing ion and pH^{λ}) represented in $\mathbf{x}_k$. The singular values s_j in the diagonal matrix $\mathbf{S}$ indicate the relative contribution of basis curve $\mathbf{u}_k$ to the observed profiles. Thus, the product $\mathbf{SV}^T$ gives the pH-dependent weight $\mathbf{w}$ applied to the individual $\%R_f$ basis curves when reconstructing the observed profiles, and therefore represents a model-independent "titration curve" for the change in the $\%R_f$ distributions (*30*):

$$w_i = s_j v_{ji}^{\mathbf{T}} \tag{7}$$

Since both $\mathbf{U}$ and $\mathbf{V}$ are unitary, $\mathbf{w}$ can be directly used to compare the relative effects of one trailing ion to another. For the dsDNA data, the $\%R_f$ line shape is dominantly represented by the first basis curve $\mathbf{u}_1$ with its correspondingly dominant singular value ($s_1 = 1354$) (Figure 7A,B; note that $\mathbf{u}_1$ appears to be "inverted" because $w_1 < 0$). The second basis curve $\mathbf{u}_2$ (Figure 7C) makes a smaller contribution ($s_2 = 192$; $s_2/s_1 = 0.14$) but is significant in the case of tricine and bicine (for which $w_2 > 0$ under all conditions; Figure 7D), reflecting the lack of dispersion in their $\%R_f$ distributions. Inspection of w_3 shows that $\mathbf{u}_3$ (and subsequent $\mathbf{u}_k$) make only a minor (and constant for all amino acids) contribution ($s_3 = 56$; $s_3/s_1 = 0.04$) to the observed $\%R_f$ curves (Figure 7E,F). We did not analyze the data for FW DNA by SVD due to the low density of data, particularly at lower pH.

Using a set of trailing ions under contrived conditions to span a range of net mobilities, Doktycz suggested that the $\%R_f$ distribution could be correlated to the net ion mobility μ_{net} (*16*). However, this cannot explain the apparent convergence of the $\%R_f$ distributions with an increase in pH, as μ_{net} values themselves do not converge with an increase in pH (Figure 4). Thus the ion-specific dispersion of the $\%R_f$ dispersion is inconsistent with a simple transport effect argued solely on the basis of conductances/mobilities of the trailing ion (*31*). On the other hand, convergence of the $\%R_f$ curves at high pH emerges naturally when expressed as a function of concentrations of N_α-protonated groups in phase π (Figure 7B,D). Thus, the ion-specific order in the dispersion of $\%R_f$ distributions (natural amino acids > bicine, tricine) can be satisfactorily explained in terms of the accumulation of N_α-protonated ions in phase π, which is in turn a function of their basicity and free mobility (Figure 3). In other words, the weaker bases tricine and bicine simply do not accumulate sufficient concentrations of N_α-protonated ions in phase π to effect the same degree of dispersion in the $\%R_f$ distributions as the natural amino acids which, being approximately equally basic, yield similar dispersions. The net ionic mobility of the trailing ion comes into play in that it is a determining factor on c_X (eq 3) and may serve as a surrogate marker for the concentration of N_α-protonated amino acids in phase π. Thus, electrostatic interactions between the $-NH^+$ group and the DNA polyanion appear to be a mass-action effect and modify the mobility of DNA analytes during electrophoresis. Although neither the lack of a mechanistic model at present nor the limits of attainable NH^+ concentration in our experiments (up to ~0.3 M; Figure 3) permit a quantitative estimation of affinity constants, inspection of the data (Figure 7B,D) suggests values no greater (and perhaps considerably lower) than 10^3 M^{-1}, consistent with values observed with simple ion pairs in solution.

Gabbay and co-workers have described the stabilization of nucleic acid duplexes by amino acids and analogues against thermal denaturation in solution (*7*, *8*, *10*). In particular, they observed by UV melting that the amino acid amides at 200 mM increased the melting temperature T_m of ribonucleic (rI-rC and rA-rU) and deoxyribonucleic (calf thymus) duplexes by ~5 °C (ΔT_m). This indicates that amino acids interact more strongly with duplex than single-stranded DNA. We observed a similar phenomenon with the self-complementary 12 bp dsDNA fragment (Figure 5A) which

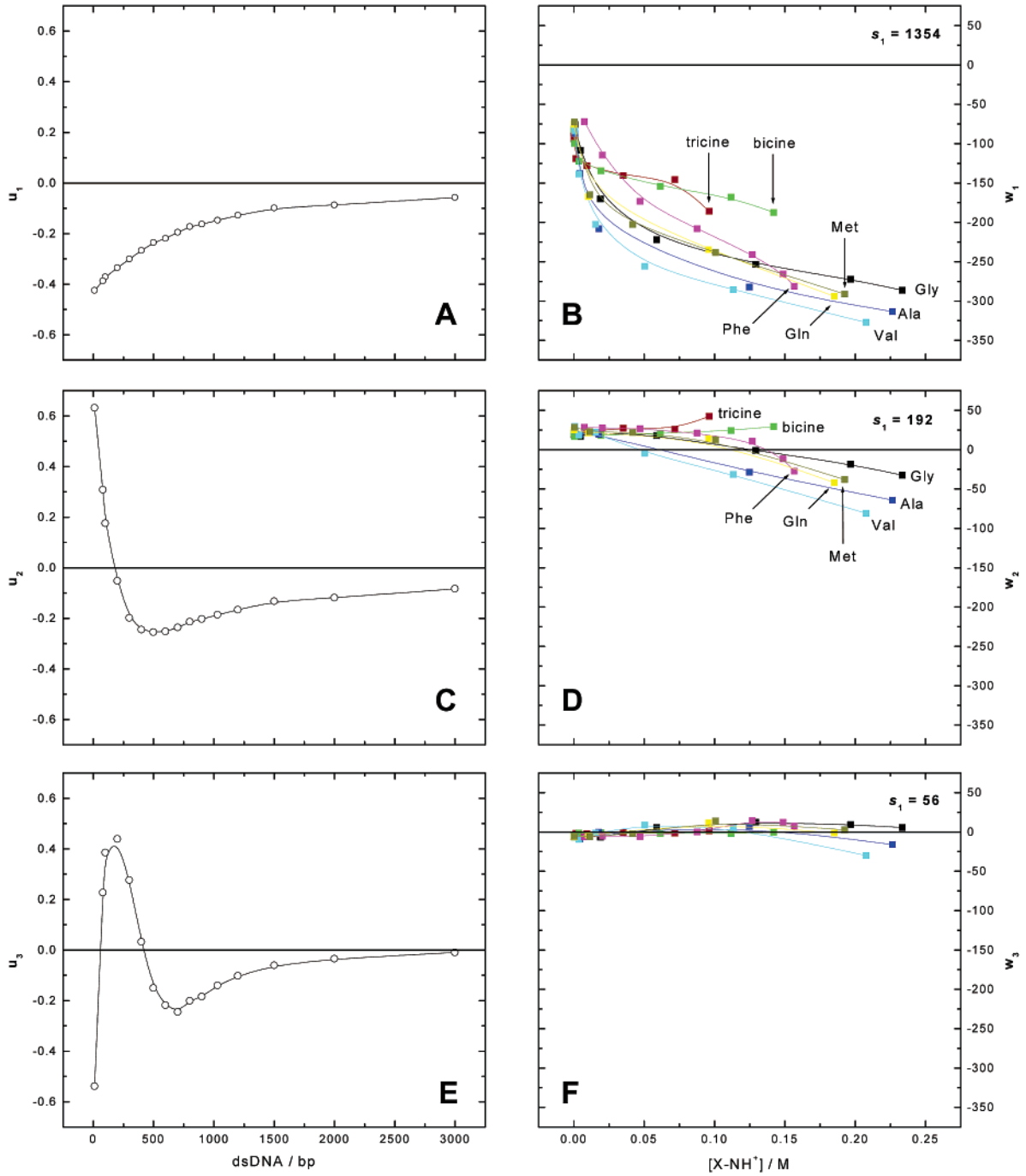

FIGURE 7: SVD analysis of dsDNA $\%R_f$ distributions. Aggregate data for dsDNA (all trailing ions) (Figure 6A) were analyzed by SVD according to eq 6. (A, C, and E) The basis $\%R_f$ curves $\mathbf{u}_1-\mathbf{u}_3$, respectively. (B, D, and F) Weighting coefficients w_1-w_3, respectively, as defined by eq 7 applied to the corresponding basis curves $\mathbf{u}_k$ to reconstruct the observed $\%R_f$ line shapes. The corresponding singular values are given. Concentrations of N_α-protonated amino acid trailing ions [X-NH$^+$] along the absicissa are as determined in Figure 3. Note that for each column of panels the ordinate is scaled identically to emphasize the relative contributions of the components. Arrows indicate titration end points reached for each trailing ion.

was significantly more retarded than its 12-nucleotide constituent strand than is expected in a common TBE gel. Moreover, Gabby and co-workers noted that the concentration of an amino acid amide required to achieve the same ΔT_m is inversely correlated with the net positive charge of the amino acid amide (*8*), in agreement with the notion that amino acids interact with nucleic acids via electrostatic interactions. DNA−amino acid interactions have also been reported in capillary electrophoresis with an isoelectric histidine running buffer (*32*).

On the basis of this proposal, we must also consider TrisH$^+$ as a source of $-NH^+$ groups, and we found that it alone had a negligible effect on the $\%R_f$ distribution. We note that an increase in $\%R_f$ as a result of association of $-NH^+$ ions is not contradictory since the absolute mobility of the analytes is almost always reduced with a decrease in pH (the advantage in distance traveled being offset by the substantially longer run times required for the moving boundary to traverse the gel). The trailing ions, whose $-NH^+$ charge is neutralized by the carboxylate in the molecule (such

that it is net neutral in this state of ionization), would predictably have a less adverse effect on the net charge and therefore mobility of the DNA analyte (compare Tris and tricine, for example, which are equally basic). The observed dispersions in the $\%R_f$ distributions therefore represent the net effect of competing interactions with N_α-protonated trailing ions and $TrisH^+$, and the narrower dispersion observed with tricine and bicine may be partly due to the higher concentrations of $TrisH^+$ in phase π (Figure 3).

The biphasic $\%R_f$ distributions observed with dsDNA are likely a manifestation of the bend persistence length (50 nm, or ~150 bp): fragments shorter than this migrate end-on as stiff rods and exhibit greater mobility than longer, entangled fragments which suffer from entropic trapping in the PAA matrix. This property appears to be preserved even as small fragments become progressively stacked with the moving boundary as the pH decreases. In the case of FW DNA, reptation analysis has shown that entropic trapping plays a significant role for assembled structures with long arms [such as $d(A_{30}G_{15})$] but not $d(A_{15}G_{15})$ in the PAA matrix used here (10% T, 2.7% C) (*23*). Thus, the $\%R_f$ distributions we obtained with $d(A_{15}G_{15})$ ODNs, particularly the small oligomers, should represent migration in the Ogston sieving régime in which analytes can be treated as globular objects whose gyration radii are smaller than the characteristic pore size of the matrix. This is consistent with our results (Figure 6B) which indicate a strictly monophasic size dependence at all pHs tested and suggest a persistence length longer than a 12-mer. That even highly oligomeric FW DNA should exhibit Ogston migration while large dsDNA reptates suggests that FW DNA has a compact and rigid hydrodynamic structure, resulting presumably from strong interactions in the guanine-rich core. Even the 30-nucleotide monomer migrates as a highly compact structure, exhibiting a higher $\%R_f$ than a non-guanine-rich 12-nucleotide fragment (Figure 5). In terms of the effects of trailing ions on $\%R_f$ dispersion, however, FW and dsDNA are fairly similar. Tricine (L_S = 2 at pH^λ 7), which also produced the slightest dispersion in the $\%R_f$ distributions for dsDNA, had a similar effect on FW DNA; bicine was intermediate (below the natural amino acids, $L_S \geq 4$ at pH^λ 7) in the sense that the stacking limit was only slightly more increased at this pH (L_S = 3). Moreover, for both isoforms, the larger fragments enjoy a greater relative increase in $\%R_f$ than smaller fragments for a given drop in pH^π. Given their structural differences from dsDNA, some peculiarities observed with FW DNA are not unexpected, but are nonetheless consistent with interactions with amino acids acting as trailing ions and their differential accumulation in phase π. Moreover, since the noncovalent FW oligomers are known to exchange strands during electrophoresis (*25*), the potential exists for N_α-protonated trailing phase constituents to complicate the FW exchange kinetics. In the aggregate, the effects of trailing ions on the electrophoretic migration of FW DNA share sufficient similarities with their effects on dsDNA that a role for interactions with N-protonated amino acids acting as trailing ions, as we have proposed for dsDNA, is reasonable and warrants further investigation.

ACKNOWLEDGMENT

We thank Ms. Diana Morarescu of MBI Fermentas for providing sequence information about the dsDNA ladder.

REFERENCES

1. Montenay-Garestier, T., and Hélène, C. (1968) Molecular interactions between tryptophan and nucleic acid components in frozen aqueous solutions, *Nature 217*, 844−845.
2. Montenay-Garestier, T., and Hélène, C. (1971) Reflectance and luminescence studies of molecular complex formation between tryptophan and nucleic acid components in frozen aqueous solutions, *Biochemistry 10*, 300−306.
3. Montenay-Garestier, T., and Hélène, C. (1973) Aggregate formation in frozen aqueous solutions of nucleic acid derivatives and aromatic amino acids. Energy transfer and complex formation, *J. Agric. Food Chem. 21*, 11−16.
4. Hélène, C., Montenay-Garestier, T., and Charlier, M. (1973) Excited-state interactions and energy transfer between aromatic amino acids and nucleic acid components, *Ann. Acad. Bras. Cienc. 45* (Suppl.), 59−62.
5. Hélène, C., Dimicoli, J. L., and Brun, F. (1971) Binding of tryptamine and 5-hydroxytryptamine (serotonin) to nucleic acids. Fluorescence and proton magnetic resonance studies, *Biochemistry 10*, 3802−3809.
6. Hélène, C., Montenay-Garestier, T., and Dimicoli, J. L. (1971) Interactions of tyrosine and tyramine with nucleic acids and their components. Fluorescence, nuclear magnetic resonance and circular dichroism studies, *Biochim. Biophys. Acta 254*, 349−365.
7. Gabbay, E. J., and Kleinman, R. W. (1970) Topography of nucleic acid helices in solutions. The interaction specificities of optically active amino acid derivatives, *Biochem. J. 117*, 247−256.
8. Gabbay, E. J., Kleinman, R., and Shimshak, R. R. (1968) Topography of nucleic acid helices in solutions. VIII. Selective interactions of L-amino acids and peptides with nucleic acid helices, *J. Am. Chem. Soc. 90*, 1927−1928.
9. Gabbay, E. J., Kleinman, R., and Shimshak, R. R. (1968) Topography of nucleic acid helices in solutions. VI. The effect of amino acid derivatives on the RNase-catalyzed hydrolysis of polyadenylic acid. Demonstration of an asymmetric surface, *Biopolymers 6*, 993−996.
10. Gabbay, E., and Kleinman, R. (1967) Topography of nucleic acid helices in solutions. V. The interactions of L-, D-, and DL-amino acid derivatives with nucleic acid helices. Demonstration of an asymmetric surface, *J. Am. Chem. Soc. 89*, 7123−7125.
11. Chen, Q., and Richardson, N. V. (2003) Enantiomeric interactions between nucleic acid bases and amino acids on solid surfaces, *Nat. Mater. 2*, 324−328.
12. Alonso, A., Martin, P., Albarran, C., and Sancho, M. (1993) Amplified fragment length polymorphism analysis of the VNTR locus D1S80 in central Spain, *Int. J. Leg. Med. 105*, 311−314.
13. Takeshita, H., Yasuda, T., Nakajima, T., Nakashima, Y., Mori, S., Mogi, K., and Kishi, K. (1999) Simultaneous typing of the STR loci, vWF and HumTPO, using discontinuous polyacrylamide gel electrophoresis, *Leg. Med. 1*, 135−139.
14. White, E., Sahota, R., and Edes, S. (2002) Rapid microsatellite analysis using discontinuous polyacrylamide gel electrophoresis, *Genome 45*, 1107−1109.
15. Sajantila, A., and Lukka, M. (1993) Improved separation of PCR amplified VNTR alleles by a vertical polyacrylamide gel electrophoresis, *Int. J. Leg. Med. 105*, 355−359.
16. Doktycz, M. J. (1993) Discontinuous electrophoresis of DNA: Adjusting DNA mobility by trailing ion net mobility, *Anal. Biochem. 213*, 400−406.
17. Jovin, T. M. (1973) Multiphasic zone electrophoresis. I. Steady-state moving-boundary systems formed by different electrolyte combinations, *Biochemistry 12*, 871−879.
18. Jovin, T. M. (1973) Multiphasic zone electrophoresis. III. Further analysis and new forms of discontinuous buffer systems, *Biochemistry 12*, 890−898.
19. Jovin, T. M. (1973) Multiphasic zone electrophoresis. II. Design of integrated discontinuous buffer systems for analytical and preparative fractionation, *Biochemistry 12*, 879−890.
20. Protozanova, E., and Macgregor, R. B., Jr. (1996) Frayed wires: A thermally stable form of DNA with two distinct structural domains, *Biochemistry 35*, 16638−16645.
21. Jovin, T. M. (1973) Multiphasic zone electrophoresis, IV. Design and analysis of discontinuous buffer systems with a digital computer, *Ann. N.Y. Acad. Sci. 209*, 477−496.
22. Protozanova, E., and Macgregor, R. B., Jr. (1998) Circular dichroism of DNA frayed wires, *Biophys. J. 75*, 982−989.

23. Protozanova, E., and Macgregor, R. B., Jr. (1998) Analysis of the electrophoretic migration of DNA frayed wires, *Biophys. Chem. 75*, 249−257.
24. Poon, K., and Macgregor, R. B., Jr. (1999) Probing the structure of multi-stranded guanine-rich DNA complexes by Raman spectroscopy and enzymatic degradation, *Biophys. Chem. 79*, 11−23.
25. Protozanova, E., and Macgregor, R. B., Jr. (1999) Transient association of the DNA-ligand complex during gel electrophoresis, *Electrophoresis 20*, 1950−1957.
26. Protozanova, E., and Macgregor, R. B., Jr. (2000) Thermal activation of DNA frayed wire formation, *Biophys. Chem. 84*, 137−147.
27. Poon, K., and Macgregor, R. B., Jr. (2000) Formation and structural determinants of multi-stranded guanine-rich DNA complexes, *Biophys. Chem. 84*, 205−216.
28. Protozanova, E., and Macgregor, R. B., Jr. (2001) Formation of DNA frayed wires is independent of the directionality of the parent strand, *Biopolymers 58*, 355−358.
29. Ornstein, L. (1964) Disc Electrophoresis. I. Background and Theory, *Ann. N.Y. Acad. Sci. 121*, 321−349.
30. Segel, D. J., Fink, A. L., Hodgson, K. O., and Doniach, S. (1998) Protein denaturation: A small-angle X-ray scattering study of the ensemble of unfolded states of cytochrome *c*, *Biochemistry 37*, 12443−12451.
31. Allen, R. C., and Doktycz, M. J. (1996) Discontinuous electrophoresis revisited: A review of the process, *Appl. Theor. Electrophor. 6*, 1−9.
32. Stellwagen, N. C., Gelfi, C., and Righetti, P. G. (1999) DNA-histidine complex formation in isoelectric histidine buffers, *J. Chromatogr., A 838*, 179−189.
33. Longsworth, L. G. (1972) Diffusion in Liquids, in *American Institute of Physics Handbook* (Gray, D. E., Ed.) 3rd ed., pp 224−226, McGraw-Hill, New York.

BI0480786